Electronic Structure

DOI: 10.1002/anie.201202560

Clar's Aromatic Sextet and π-Electron Distribution in Nanographene**

Shintato Fujii and Toshiaki Enoki**

Graphene, which consists of an infinite number of benzene rings fused together, has attracted intensive research interest in physics, mostly because of its unique electronic properties, such as the anomalous quantum Hall effect[1] and Klein tunneling,[2] which are a consequence of massless Dirac fermions with linear energy dispersions near the Fermi level in the electronic band structure.[3] When an infinite graphene sheet is cut into nanosized fragments (nanographene) having open edges, the nanosize effect on the electronic structure is of particular interest. At the nanometer scale, electronic properties are significantly dependent on the size and edge shape.[4,5] In contrast to infinite-sized graphene, in which all the π electrons are uniformly distributed over the honeycomb carbon network (see Figure S1 in the Supporting Information), the presence of edges in nanographene gives rise to unconventional features in the electronic structure and as a consequence unique electronic and magnetic properties are induced in the system. There are two typical graphene edge terminations, that is, armchair and zigzag (Figure S1 C). For example, triangular-shaped graphene fragments terminated by zigzag edges, such as phenalenyl derivatives, feature a spin-polarized open-shell structure in the ground state, which is expected to be employed as a spin carrier in future electronic devices.[6] In contrast, armchair-terminated graphene fragments such as triphenylene derivatives do not support such unique properties, but instead feature higher energy stabilization resulting from a larger HOMO–LUMO (highest occupied molecular orbital—lowest unoccupied molecular orbital) gap. For small polycyclic aromatic hydrocarbons (PAHs) having a size of a few nanometers, Clar's theory[7] has proven to be a model for the edge-shape-dependent π-electron distribution. There have been several efforts made to apply this theory to nanosized graphene systems such as carbon nanotubes,[8,9] graphene nanoribbons,[10,11] and nanographene.[12] However, experimental characterization is still lacking, partially because of the difficulty in preparing nonbenzenoid graphene systems, which are expected to be highly reactive.[13] The successful preparation and characterization of nanosized graphene systems has been mostly limited to full benzenoid systems.[14,15] Herein we investigate the electronic properties of finite-sized nanographene fragments consisting of approximately several tens of fused benzene rings using conductive atomic force microscopy (AFM). Nanographene fragments are prepared by oxidizing graphene sheets, in which nanosized graphene domains are isolated by oxidized sp^3-carbon backbones. The rather harsh oxidation conditions lead to the formation of various nanographene systems, including full, partial, or nonbenzenoid systems. This process has allowed investigation and interpretation of the geometry-dependent electronic properties of nanographene systems with the assistance of Clar's theory. In recent years, oxidized graphene has emerged as a solution-processable material for large-area electronic devices[16] because it can be readily functionalized and deposited on a variety of substrates.[17–20] However, limited knowledge of the nanoscale electronic properties has hindered improvement of the device performance. Therefore, one of the objectives of the present study is to provide a better understanding of the electronic properties of the nanographene system. Herein, we first present the structural and electronic characterization of the nanographene fragments in the oxidized graphene sheets using noncontact AFM (NC-AFM) imaging. We then focus on size-dependent electron transport though metal/nanographene/metal junctions created by contact AFM, and correlate it to size-dependent electronic gap structures of the nanographene fragments. Next, Clar's theory is introduced, and its applicability to the prediction and explanation of edge-shape-dependent π-electron distributions (i.e. nanoscale spatial variation of the charge-transport properties) in nanographene fragments is discussed. Finally, we present data from high-resolution conductive-AFM studies of the π state of nanographene and correlate them to the edge shape with the assistance of Clar's theory.

Figure 1 A shows an NC-AFM image of an oxidized graphene sheet with a lateral size of approximately 200 × 200 nm^2. For details of the experimental setup, see the Supporting Information. According to extensive studies (nuclear magnetic resonance spectroscopy, infrared spectroscopic, and electron diffraction) the COOH, OH, and C=O groups are present at the edge, while the basal plane is covered with mostly epoxide and OH groups[21] (Figure 1 C). Information on the surface distribution of oxygen-containing functional groups can be obtained from tunneling current mapping during the NC-AFM imaging (Figure 1 B), wherein nanosized regions having higher tunneling current are evident. The conductive regions are attributable to pristine graphene fragments isolated by oxidized regions, which can be thought of as two-dimensional π-electron systems confined

[*] Dr. S. Fujii, Prof. T. Enoki
Department of Chemistry, Tokyo Institute of Technology
2-12-1 Ookayama, Meguro-ku, Tokyo 152-8551 (Japan)
E-mail: fujii.s.af@m.titech.ac.jp
enoki.t.aa@m.titech.ac.jp

[**] This work was supported by Grants-in-Aid for Scientific Research (No. 20001006 & No. 23750150) from the Ministry of Education, Culture, Sports, Science and Technology of Japan.

Supporting information for this article is available on the WWW under http://dx.doi.org/10.1002/anie.201202560.

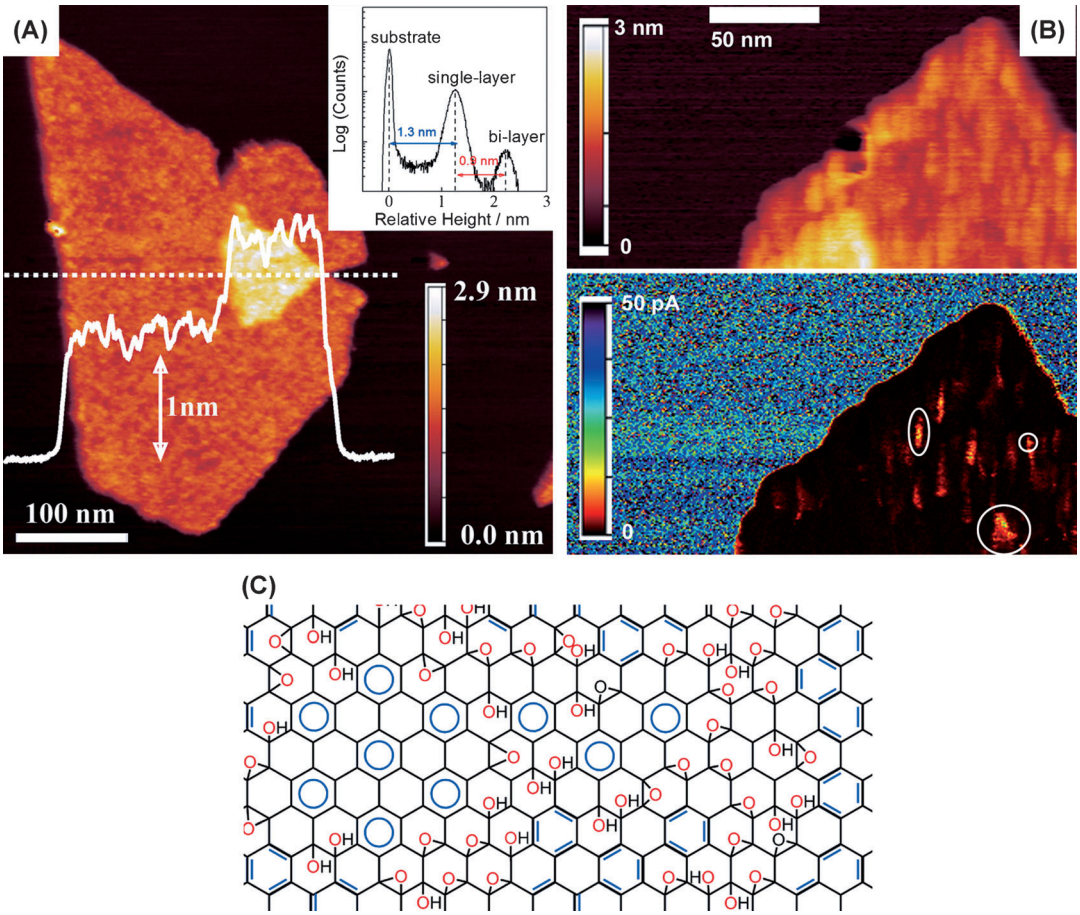

Figure 1. AFM images of oxidized graphene sheets and a structural model. A) NC-AFM image of an oxidized graphene sheet on HOPG with a height profile acquired along the dotted line (z scale bar = 1 nm). The height histogram (inset) reveals that the sheet thickness between the bilayer and single-layer regions is ca. 0.9 nm. The increased thickness over that of graphene (ca 0.3 nm) is due to partial modification of the original sp^2 carbon atoms into sp^3 carbon atoms by attachment of oxygen-containing functional groups. B) Simultaneously measured NC-AFM topography (upper) and tunneling current (lower) image of another oxidized graphene on HOPG; several graphene fragments are indicated by white circles in the current image. C) Structural model of oxidized graphene, in which the basal plane is mostly modified by OH and epoxide functional groups. The sextet positions in the nanographene fragments can be identified only when their edge structures are known. Therefore sextet positions of the two nanographene fragments at the center are drawn in this model. Imaging conditions for (A): cantilever = NSC11, frequency shift (Δf) = −10 Hz, V_b = 0 V; for (B): cantilever = NSC11/Pt, Δf = −15 Hz, V_b = +0.10 V.

within nanoscale spaces. The presence of such isolated nanosized graphene fragments has recently been identified by high-resolution transmission electron microscopic (TEM) studies of oxidized graphene sheets.[22,23] However, apart from such crystallographic characterization, electronic characterization on the atomic scale is considerably lacking. In this study, electronic characterization is realized by high-resolution current mapping of metal/nanographene/metal junctions created by the contact AFM setup.

Figure 2 A shows a current-mapping image of patches of nanographene fragments in oxidized graphene, and larger nanographene fragments indicate higher tunneling current (see the lower panel in Figure 2 A). This result is attributable to size-dependent effective tunneling barriers of the nanographene junctions. Charge transport through molecule junctions sandwiched by metal electrodes has been successfully explained by a molecular-orbital-mediated tunneling barrier model.[24] In this model, charge transport is described by charge tunneling through an effective barrier that is associated with an energy level alignment between the Fermi level of metal electrode(s) and frontier orbital(s) of a molecule in a junction (see the Supporting Information and Figure S2 A). HOMO–LUMO gaps (and/or closest lying molecular orbital with respect to Fermi level of metal electrodes) have been reported to have a linear correlation to the effective tunneling barrier height. Because HOMO–LUMO gaps monotonically decrease with increasing the size of a homogeneous series of nanographene, the observed monotonic increase of tunneling current, that is, a decrease in effective barrier heights, can be understood by a size-dependent gap-closing nature (Figure S2 B). The gap-closing nature can be intuitively explained by the development of molecular orbitals and a decrease in the energy level differences between neighboring orbitals having an increasing number of atoms based on the theory of linear combination of atomic orbitals (LCAO) of π-electron systems.[13,25–27] Therefore the larger nanographene has a higher tunneling probability (i.e. lower effective tunneling barrier)[24,28–31] because of the

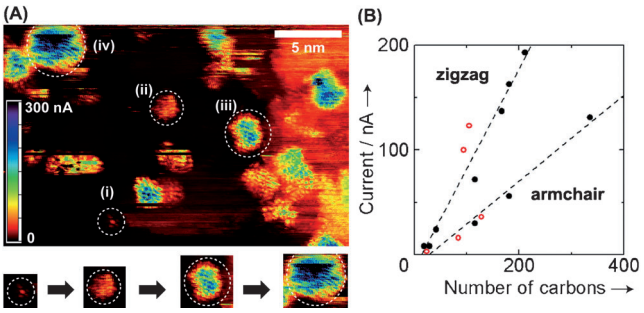

Figure 2. A) Observed π state for nanographene fragments in oxidized graphene on Au(111) ($V_b = 0.15$ V), in which a size distribution from ca. 1 to 5 nm is apparent; some are marked by dotted circles. Higher tunneling current was observed for larger nanographene fragments, as shown in the lower panel. B) Tunneling currents for nanographene fragments from the image in Figure 2A against the number of carbon atoms (filled circles). The open circles correspond to currents for the nanographene fragments shown in Figures 4A and 5A—D. There are two distinguishable distributions having different slopes, which could indicate the edge-shape-dependent gap closing predicted for zigzag- or armchair-terminated nanographene (for details, see the main text.).

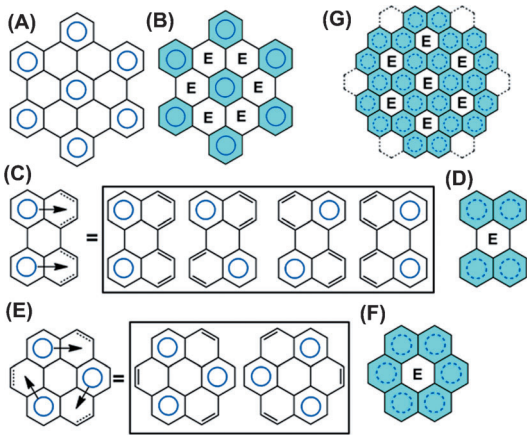

Figure 3. A) Clar formula for HBC. B) Localized sextet (π electron) distribution with $\sqrt{3} \times \sqrt{3}R30^\circ$ periodicity for HBC. Empty rings are indicated by "E". C) Clar formula for perylene, in which sextet migration is indicated by arrows. The formula can be decomposed into four resonant Clar representations. D) Delocalized sextet distribution for perylene, which is represented by doted circles. E) Clar formula for coronene and its two resonant Clar representations. F) Circular sextet distribution for coronene. G) Circular sextet distribution for fused coronene structure with inverted $\sqrt{3} \times \sqrt{3}R30^\circ$ periodicity (i.e. $\sqrt{3} \times \sqrt{3}R30^\circ$ periodicity of empty rings).

smaller electronic gap.[29] In Figure 2B, the observed tunneling currents are plotted against the number of carbon atoms in the nanographene fragments (filled circles). This plot features 1) the expected general trend of current increase (i.e. electronic gap closing) with the increase in size, and 2) the two unexpected but distinguishable distributions having different slopes, which could indicate the edge-shape-dependent gap closing predicted for zigzag- or armchair-terminated nanographene.[25–27] In the final discussion, we will recall this edge-shape-dependent gap closing in combination with the identification of the edge types predicted from the observed π-state distributions based on Clar's theory.

Before going into a detailed characterization of the edge-dependent π state (i.e. nanoscale spatial variation of the charge-transport properties of nanographene), we introduce Clar's theory to consider edge-shape-dependent π state of the nanographene fragments. As an extension to model of the Kekulé structure, Clar's theory introduces the Clar sextet, a representation of the delocalization of six π electrons resulting from the resonance of two complementary, hexagonal Kekulé configurations (see Figure S1A in Supporting Information). According to Clar's rule, for a given geometry of fused benzene rings, the representation with a maximum number of Clar sextets (the Clar formula) is the most representative.[7] The Clar formula has proven to be an intuitive yet adequate model for predicting 1) the edge-shape-dependent π-electron distribution and 2) the most thermodynamically stable bond configurations.[32,33] This predictive ability is because the Clar formula having n Clar sextets represents the resonance of 2^n Kekulé formulas, and therefore, maximizing the number of Clar sextets is equivalent to maximizing the number of resonant Kekulé formulas in one Clar representation.[7,33] For instance, the Clar formula of hexa-peri-hexabenzocoronene (HBC), consisting of 13 peri-fused benzene rings terminated by armchair edges (Figure 3A), can be depicted by seven sextets without any localized double bonds. Such a Clar formula, represented by sextets only, indicates higher thermodynamic stability and is referred to as a full benzenoid PAH molecule in Clar's theory.[7] Note that infinite-sized graphene can be represented by three equivalent Clar formulas, and thus π electrons are distributed uniformly in the system because of sextet migration (Figure S1B), but the presence of edges, that is, the finite-sized effect in HBC, where the edges are described entirely by armchair edges, prohibits sextet migration, and hence localized sextets (π-electron distribution) having $\sqrt{3} \times \sqrt{3}R30^\circ$ periodicity with respect to the A (or B) graphene hexagonal sublattice (Figure S1B) appears in this system. In contrast, nanographene terminated by zigzag edges can be represented by anisotropic sextet migration such as linear and circular migration in perylene- (acene-) and coronene-like structures (Figures 3C,E). The sextet migration is indicative of quasilocalized double bonds (denoted by dotted bonds in Figures 3C,E), less thermodynamic stability, and a chemically more reactive nature according to Clar's theory.[7] Note that the sextet migration in the finite-sized graphene system reflects the presence of reactive localized double bonds. This is not the case in infinite-sized graphene, in which the system can be described by sextets only, but sextet migration is allowed because of the infinite-size effect without edge boundaries (i.e. periodic boundary conditions in the crystal; see arrows in Figure S1B). In this way, the presence of the edges modulates the original uniform sextet distribution in graphene and leads to inhomogeneous π-electron distribution described by localization and migration of sextets in Clar's formula for armchair- and zigzag-terminated nanographene, respectively. The localization of sextets (π electron) in the Clar formula has been experimentally identified by a scanning tunneling microscopy (STM) characterization of a full benzenoid HBC molecule[34] terminated by armchair edges. Although

experimental characterization is still lacking, it has been theoretically demonstrated that Clar's formulas of nonbenzenoid graphene nanoribbons terminated by zigzag-like edges could give rise to their STM patterns.[11] Figure 4A shows a high-resolution image of the π state for one nanographene fragment in oxidized graphene, and the $\sqrt{3} \times \sqrt{3}R30^\circ$ pattern with respect to the graphene unit cell is apparent (Figure 4B). This result is in excellent agreement with the predicted

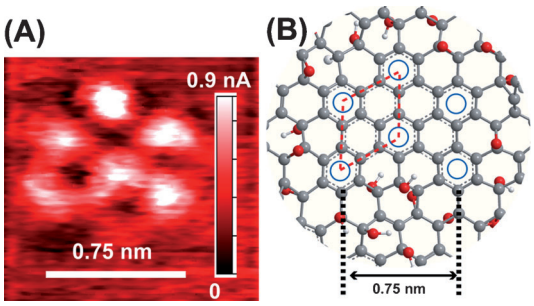

Figure 4. A) Observed π state for full benzenoid nanographene fragment. B) Proposed schematic model (C gray, O red, H white). Dotted red lines indicate the $\sqrt{3} \times \sqrt{3}R30^\circ$ pattern with respect to the graphene unit vectors. Next-neighbour distance of the sextets is ca. 0.75 nm ($3a$, $a = 0.25$ nm).

pattern of the localized sextets as is previously reported in the literature.[34] Historically similar larger periodicity (ca. 0.3–0.4 nm) relative to that of the graphene unit cell (ca. 0.25 nm) has also been observed in STM studies of three-dimensional amorphous carbon materials and ascribed to the crystalline order of stacked graphene layers (i.e. interlayer distance of 0.34 nm).[35] However, this interpretation is not applicable to the present case, because we are only studying a single-layered graphene sheet.

Herein we present a detailed characterization of the observed π-state distributions, which can be basically classified into four types. Type I is a localized sextet distribution with $\sqrt{3} \times \sqrt{3}R30^\circ$ periodicity (Figure 4A and Figure 5A) in armchair-terminated nanographene (Figure 4B), which is indicative of higher thermodynamic stability. Type II is a linear distribution along the zigzag direction (Figure 5B), which results from sextet migration in the acene-like structure terminated by zigzag edges (Figure 3D). Type III is an inverted $\sqrt{3} \times \sqrt{3}R30^\circ$ periodicity (Figure 5C), which is caused by circular sextet migration in the coronene-like structure terminated by zigzag edges (Figures 3F,G). A sextet in a hexagonal carbon network basically migrates along three zigzag directions, which reflects the threefold symmetry of the graphene sublattice. However, depending on the edge shapes, isotropic circular migration is possible. Type IV is an anisotropic distribution (Figure 5D) resulting from sextet migration in nanographene with an ill-defined structure terminated predominantly by zigzag edges, in which the complex patterns prevent assignment of the structural models. The sextet migrations in Types II–IV imply the presence of quasilocalized double bonds (see Figures 3C,E), and therefore lower thermodynamic stability is expected. In Clar's theory, the

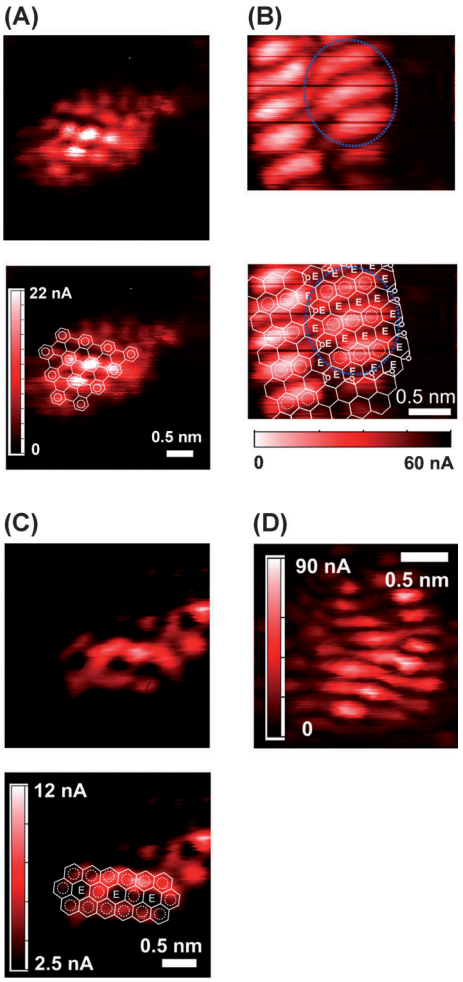

Figure 5. High-resolution imaging of the π state for nanographene in the same oxidized graphene sheet using the same AFM tip (Figure 2A and 4A) and a schematic model for Type I (A) nanographene terminated by armchair edges, Type II (B), Type III (C), and Type IV (D) for nanographene terminated by zigzag edges. The localized and migrating sextets are represented by solid and dotted circles, respectively. "E" is the empty ring (see Figure 3).

localization and migration of sextets in PAH molecules are also strongly correlated with the chemical reactivity (kinetic stability).[7] For example, lower chemical reactivity is suggested to imply a larger HOMO–LUMO gap because it is energetically unfavorable to add electrons to a high-lying LUMO or to extract electrons from a low-lying HOMO in a molecule with a larger HOMO–LUMO gap. Clar has observed that PAH molecules represented by sextet migration exhibit higher chemical reactivity, which was correlated with their smaller electronic gap structure. Nanographene fragments terminated by zigzag edges feature sextet migration and therefore a smaller electronic gap is expected. To date, there have been corresponding theoretical attempts to predict edge-shape-dependent gap closing.[25–27] In Figure 2B, we added plots of the observed current data against the number of the carbon atoms of nanographene fragments in Figure 5. Interestingly, the armchair-terminated nanographene exhibits a slower tunneling-current-increase with

increasing sizes compared to that of zigzag-terminated nanographene (see red open circles and dotted lines in Figure 2B), and is in agreement with theoretical prediction that the HOMO–LUMO gap (i.e. tunneling probability) of armchair-terminated nanographene gradually decreases relative to that of zigzag-terminated nanographene as the system size tends to infinity.[25–27] To conclude our preliminary results, statistical analyses of the tunneling current measurements across different samples is necessary, but, in general, quantitative comparison of current density of molecular junctions prepared in different samples is difficult because it is dependent upon the tip size, which is changeable during measurements. To minimize this effect, we focused on the current-mapping data with nanometer-scale resolution obtained by the same AFM probe for analyzing the size- and edge-shape-dependent tunneling probability. In these measurements, nanographene fragments with different sizes and edge shapes are prepared in one sample of oxidized graphene and we could compare their tunneling probabilities with the assumption that the tip shape is nearly constant and ideally sharp enough to resolve the nanometer scale variations in currents.

It should be noted that direct imaging of molecular orbitals with higher spatial resolution has been reported for small PAH molecules using STM.[36–38] In these studies, the STM tip is not in contact with the molecule on the substrate and higher bias voltage of ± 1–2 V was applied to set the Fermi level of metal electrodes closer to that of the molecular orbital of PAH molecules. At the higher bias regime, instead of an off-resonant tunneling process through tunneling barriers modeled in our study, a (near-)resonant tunneling process through the molecular orbital[39] is likely to dominate the transport process. These differences in 1) the configurations of the molecule junctions with and without vacuum gap and 2) the tunneling processes could lead to variations in appearance of the observed π states.

Clar's sextets essentially induce π-electron distribution patterns with $\sqrt{3} \times \sqrt{3}R30^\circ$ periodicities (see Figures 3B,G). Similar $\sqrt{3} \times \sqrt{3}R30^\circ$ periodicities have often been observed in STM studies[40] of edges (or defects) of bulk graphene, and the origin has been ascribed to edge-induced modulation of bulk electronic states at the Fermi level.[41] In this picture in solid-state physics, plane waves that are uniquely determined by the K (K′) points in the first Brillouin zone propagate into space, but the presence of the edge leads to elastic scattering of the electron wave. The armchair edge is subject to intervalley scattering between the K (K′) and K′ (K) points. Thus the incident K (K′) and reflected K′ (K) states cause interference of electron waves, thus resulting in a standing-wave state[42] with $\sqrt{3} \times \sqrt{3}R30^\circ$ periodicities. The sextet localization near the armchair edges can be explained by 1) geometrical consideration in the chemical structure represented by the Clar formula (i.e. π-bond arrangement) and 2) boundary conditions of electron waves at the edges in the bipartite lattice. The understanding of these two simple edge-induced electronic properties from the chemical and physical perspectives principally share the same origin which relates to the unique honeycomb (bipartite) lattice. However, there is still no clear direct correlation between these, so that this remains to be clarified in future study.

Received: April 2, 2012
Published online: May 29, 2012

Keywords: electronic structure · graphene · oxidation · scanning probe microscopy · surface analysis

[1] K. S. Novoselov, Z. Jiang, Y. Zhang, S. V. Morozov, H. L. Stromer, U. Zeitler, J. C. Maan, G. S. Boebinger, P. Kim, A. K. Geim, *Science* **2007**, *315*, 1379.
[2] C. W. J. Beenakker, *Rev. Mod. Phys.* **2008**, *80*, 1337–1354.
[3] A. K. Geim, K. S. Novoselov, *Nat. Mater.* **2007**, *6*, 183–191.
[4] M. Fujita, K. Wakabayashi, K. Nakada, K. Kusakabe, *J. Phys. Soc. Jpn.* **1996**, *65*, 1920–1923.
[5] K. Kusakabe, M. Maruyama, *Phys. Rev. B* **2003**, *67*, 092406.
[6] Y. Morita, S. Suzuki, K. Sato, T. Takui, *Nat. Chem.* **2011**, *3*, 197–204.
[7] E. Clar, *The Aromatic Sextet*, Wiley, **1972**.
[8] J. L. Ormsby, B. T. King, *J. Org. Chem.* **2004**, *69*, 4287–4291.
[9] M. Baldoni, D. Selli, A. Sgamellotti, F. Mercuri, *J. Phys. Chem. C* **2009**, *113*, 862–866.
[10] T. Wassmann, A. P. Seitsonen, A. M. Saitta, M. Lazzeri, F. Mauri, *Phys. Rev. Lett.* **2008**, *101*, 096402.
[11] T. Wassmann, A. P. Seitsonen, A. M. Saitta, M. Lazzeri, F. Mauri, *J. Am. Chem. Soc.* **2010**, *132*, 3440–3451.
[12] M. D. Watson, A. Fechtenkötter, K. Müllen, *Chem. Rev.* **2001**, *101*, 1267–1300.
[13] S. Müller, K. Müllen, *Philos. Trans. R. Soc. London Ser. A* **2007**, *365*, 1453–1472.
[14] J. Cai, P. Ruffieux, R. Jaafar, M. Bieri, T. Braun, S. Blankenburg, M. Mouth, A. P. Seitsonen, M. Saleh, X. Feng, K. Müllen, R. Fasel, *Nature* **2010**, *466*, 470–473.
[15] M. Treier, C. A. Pignedoli, T. Laino, R. Reiger, K. Müllen, D. Passerone, R. S. Fransel, *Nat. Chem.* **2011**, *3*, 61–67.
[16] S. Pang, Y. Hernandez, X. Feng, K. Müllen, *Adv. Mater.* **2011**, *23*, 2779–2795.
[17] Y. Zhu, S. Murali, W. Cai, X. Li, J. W. Suk, J. R. Potts, R. S. Ruoff, *Adv. Mater.* **2010**, *22*, 3906–3924.
[18] K. P. Loh, Q. Bao, P. K. Ang, J. Yang, *J. Mater. Chem.* **2010**, *20*, 2277–2289.
[19] G. Eda, M. Chhowalla, *Adv. Mater.* **2010**, *22*, 2392–2415.
[20] X. Huang, Z. Yin, S. Wu, X. Qi, Q. He, Q. Zhang, Q. Yan, F. Boey, H. Zhang, *Small* **2011**, *7*, 1876–1902.
[21] D. R. Dreyer, S. Park, C. W. Bielawski, R. S. Ruoff, *Chem. Soc. Rev.* **2010**, *39*, 228–240.
[22] N. R. Wilson, A. Pandey, R. Beanland, R. J. Young, I. A. Kinloch, L. Gong, Z. Liu, K. Suenaga, J. P. Rourke, S. J. York, J. Sloan, *ACS Nano* **2009**, *3*, 2547–2556.
[23] K. Erickson, R. Erni, Z. Lee, N. Alem, W. Gannet, A. Zettl, *Adv. Mater.* **2010**, *22*, 4467–4472.
[24] J. M. Beebe, B. Kim, J. W. Gadzuk, C. D. Frisbie, J. G. Kushmerick, *Phys. Rev. Lett.* **2006**, *97*, 026801.
[25] S. E. Stein, R. L. Brown, *J. Am. Chem. Soc.* **1987**, *109*, 3721–3729.
[26] Y. Ruiz-Morales, *J. Phys. Chem. A* **2002**, *106*, 11283–11308.
[27] A. Kuc, T. Heine, G. Seifert, *Phys. Rev. B* **2010**, *81*, 085430.
[28] J. M. Beebe, V. B. Engelkes, L. L. Miller, C. D. Frisbies, *J. Am. Chem. Soc.* **2002**, *124*, 11268–11269.
[29] J. M. Beebe, B. Kim, C. D. Frisbie, J. G. Kushmerick, *ACS Nano* **2008**, *2*, 827–832. See the Supporting Information.
[30] H. Song, Y. Kim, Y. H. Jang, H. Jeong, M. A. Reed, T. Lee, *Nature* **2009**, *462*, 1039–1043.
[31] B. Kim, S. H. Choi, X. Y. Zhu, C. D. Frisbie, *J. Am. Chem. Soc.* **2011**, *133*, 19864–19877.
[32] T. M. Krygowski, M. K. Cyrański, *Chem. Rev.* **2001**, *101*, 1385–1419.

[33] M. Randić, *Chem. Rev.* **2003**, *103*, 3449 – 3605.
[34] I. Gutman, Ž. Tomović, K. Müllen, J. P. Rabe, *Chem. Phys. Lett.* **2004**, *397*, 412 – 416.
[35] N. H. Cho, D. K. Veirs, J. W. Ager III, M. D. Rubin, C. B. Hopper, D. B. Bogy, *J. Appl. Phys.* **1992**, *71*, 2243 – 2248.
[36] J. Repp, G. Meyer, S. M. Stojković, A. Gourdon, C. Joachim, *Phys. Rev. Lett.* **2005**, *94*, 026803.
[37] W. H. Soe, C. Maezono, A. De Sarkar, N. Chendrasekhar, C. Joachim, *Phys. Rev. Lett.* **2009**, *102*, 176102.
[38] H. T. Zhou, J. H. Mao, G. Li, Y. L. Wang, X. L. Feng, S. X. Du, K. Müllen, H.-J. Gao, *Appl. Phys. Lett.* **2011**, *99*, 153101.
[39] T. Böhme, C. D. Simpson, K. Müllen, J. P. Rabe, *Chem. Eur. J.* **2007**, *13*, 7349 – 7357.
[40] K.-i. Sakai, K. Takai, K.-i. Fukui, T. Nakanishi, T. Enoki, *Phys. Rev. B* **2010**, *81*, 235417.
[41] G. M. Shedd, P. E. Russell, *Surf. Sci.* **1992**, *266*, 259 – 264.
[42] K. Sasaki, K. Wakabayashi, T. Enoki, *New J. Phys.* **2010**, *12*, 083023.

